ЖУРНАЛ СТРУКТУРНОЙ ХИМИИ

2011. Том 52, № 4 *Июль – август* *С. 696 – 703*

UDC 541.6:546.97:546.72.74

FIRST-PRINCIPLES STUDY ON THE MRh_{12} (M = Rh, Fe, Co, AND Ni) CLUSTERS

© 2011 **X. Kuang[1,2]*, X. Wang[1], G. Liu[1]**

[1]*College of Mathematics and Physics, Chongqing University, Chongqing, 400044, China*
[2]*School of Science, Southwest University of Science and Technology, Mianyang, Sichuan, 621010, China*

Received September, 3, 2010

In this paper, a first-principles study on the stability, electronic and magnetic properties of MRh_{12} (M = Rh, Fe, Co and Ni) clusters is performed. By optimizing the geometrical structure, we find that MRh_{12} clusters change from a perfect icosahedron to a distorted structure and have an obvious bond length contraction as compared with the corresponding bulk phase; $FeRh_{12}$, $CoRh_{12}$, and $NiRh_{12}$ clusters are more energetically stable than the $RhRh_{12}$ cluster. The effect of the impurity M on the density of states, valence band width, HOMO and LUMO for MRh_{12} clusters is not significant, but when the central Rh atom is substituted with M, the magnetic moment of MRh_{12} reduces dramatically. The Mulliken population analysis indicates that there are more charge transfers from other orbitals to Rh4*d* and M3*d* orbitals, and the *spd* hybrid effect in *d* orbitals of MRh_{12} clusters is stronger than that in the $RhRh_{12}$ cluster. this situation means that the unpaired *d* electrons have more chance to be paired, and the magnetic moments of MRh_{12} clusters can be reduced reasonably.

K e y w o r d s: MRh_{12} cluster, geometrical structure, electronic and magnetic properties.

INTRODUCTION

Small transition metal (TM) clusters is an active research area not only because such clusters have some intrinsic electronic, optical, magnetic, and structural properties different from their bulk counterparts, but also because they may serve as a model for understanding localized electronic phenomena in metals. It is also fundamentally important for us to explore new cluster-based materials with uncommon properties.

Many theoretical calculations and experimental measurements have been conducted for TM clusters [1—11]. Both theoretical and experimental studies [7—11] for small Fe, Co, and Ni clusters have shown that these clusters had larger average magnetic moment per atom than atoms in the bulk phase. Moreover, using the local spin density function theory, Reddy *et al*. first proposed theoretically that 13-atom clusters of Pd, Rh, and Ru were magnetic [12]; then Cox *et al.* observed [13, 14] experimentally giant magnetic moment in small Rh clusters. This enhancement of magnetism in small clusters can be qualitatively understood as a consequence of the reduction of local coordination number, which results in a stronger localization of 3*d* electron states and in a reduction of the effective *d* band width. Apart from the homo-atomic clusters, in order to increase the number of variables for the purpose of material design and control, some doped clusters composed of two or more elements have also been studied extensively in the recent years [15—20]. The properties of doped clusters depend not only on the cluster size and geometry, but also on the cluster composition [15—20]. Heterogeneous clusters are expected to show an extremely rich variety of magnetic behaviors as a function of the composition and chemical order [15—20]. Some calculations on bimetallic clusters have been performed by the DFT method [21—24]. These researches indicate that the impurity atoms can strongly

* E-mail: xkdkxj@yahoo.com.cn

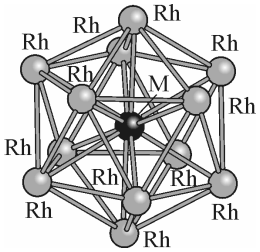

Fig. 1. Initialization geometric structure of MRh_{12} cluster

affect the geometric, electronic, and magnetic properties of mixed clusters. Recent experimental studies [25, 26] have also shown that bimetallic Co—Rh nanoparticles presented the average magnetic moment per atom that was remarkably enhanced with respect to macroscopic Co—Rh alloys of similar concentrations. These systems are therefore very good candidates for highly stable magnetic clusters and have great advantage for potential technological applications. Consequently, a systematic deep insight in the properties of mixed TM clusters seems to be very worthwhile.

In this paper, we perform a comprehensive first-principles study on MRh_{12} (M = Fe, Co, and Ni) clusters, in order to investigate the effect of the impurity M on the stability, electronic and magnetic properties. We also calculated the same properties for the $RhRh_{12}$ cluster by the same method and parameters. The paper is arranged as follows: the cluster model and computational method are described in the second part; calculation results and discussion are presented in the third part; finally, we summarize the main conclusions in the last part.

COMPUTATIONAL METHOD AND CLUSTER MODEL

The geometrical and electronic structure and magnetic properties of MRh_{12} clusters are calculated using the Vienna *ab initio* simulation program (VASP) developed at the Institute of Materialphysik of the University of Vienna, which solves the spin-polarized self-consistent Kohn-Sham equations within the projector augmented wave (PAW) method. This allows a considerably improved efficiency in terms of computation time.

The exchange-correlation effects have been described by means of the generalized gradient approximation (GGA) Perdew-Wang 91 function (PW91) under the density function theory, which is a reasonably good approximation for the calculation of cluster ground state properties. The used plane-wave energy cut-off is 14.7 Ha. For isolated clusters, we consider a supercell size of about 1.0 ~ 1.5 nm, which has been checked to ensure that the interactions between the adjacent clusters are negligible. All initial structures are fully optimized by relaxing the atomic positions until forces acting on each atom vanished (typically, $|F_i| \le 0.002$ Ha/Å) and by maximizing the binding energy.

Since the exact structure of the 13-atom cluster is not available experimentally and the number of possible geometries increases quite rapidly with cluster size, it is very difficult to determine the ground-state structures of the cluster. However, some previous studies [27, 28] on TM clusters have shown that the icosahedral structure is the most energetically stable for a 13-atom Rh cluster. We chose the icosahedral point-group symmetry with M at the center of the icosahedron as the initial structure of MRh_{12}. During the calculation, the symmetry of the initial structure was unrestricted. The geometry of the icosahedral MRh_{12} cluster is shown in Fig. 1.

RESULTS AND DISCUSSION

First, we optimized the geometrical structures of MRh_{12} clusters. Because the initial geometrical structures are unrestricted, some changes in the cluster structures have taken place during the optimization. For convenience of expression, we divided the interatomic distances of the optimized geometrical structures into four types: the equilibrium bond length among the upper (lower) pentagon atoms; the equilibrium bond length between the upper (lower) peak atom and the upper (lower) pentagon atoms; the equilibrium bond length between the central M atom and the upper (lower) pentagon atoms; the equilibrium bond length between the central M atom and the upper (lower) peak atom. We designated them as R_1, R_2, R_3, and R_4 respectively. The calculation results for these four types of the interatomic distances are listed in Table 1.

Before optimization, all these interatomic distances are equal in one cluster. The cluster structures are a perfect icosahedron with the I_h symmetry. After optimization, from the data listed above, we can

Table 1

Equilibrium interatomic distances and binding energy for MRh_{12} *clusters*

Cluster	R_1, nm	R_2, nm	R_3, nm	R_4, nm	$R_{M—Rh}$, nm	E_b, eV
$RhRh_{12}$	0.2652	0.2686	0.2590	0.2728	0.2612	52.641
	0.2654	0.2686	0.2589			
	0.2653	0.2687	0.2590			
	0.2653	0.2687	0.2591			
	0.2654	0.2687	0.2589			
$RhFe_{12}$	0.2621	0.2651	0.2555	0.2682	0.2576	73.765
	0.2622	0.2652	0.2556			
	0.2622	0.2652	0.2556			
	0.2621	0.2651	0.2555			
	0.2621	0.2652	0.2556			
$RhCo_{12}$	0.2596	0.2663	0.2537	0.2738	0.2571	65.706
	0.2599	0.2664	0.2536			
	0.2599	0.2663	0.2537			
	0.2596	0.2666	0.2540			
	0.2596	0.2666	0.2540			
$RhNi_{12}$	0.2639	0.2674	0.2586	0.2727	0.2605	75.432
	0.2640	0.2674	0.2582			
	0.2641	0.2675	0.2579			
	0.2641	0.2673	0.2582			
	0.2640	0.2675	0.2579			

easily find that the difference in the same type of the interatomic distances in one cluster is very small and can be neglected, but the difference between different types of the interatomic distances in the same cluster is obvious and can not be neglected. The cluster structure changed from the I_h symmetry to D_{5h} symmetry. According to the Jahn—Teller theorem, it is reasonable that MRh_{12} clusters have the tendency to further distortion to lower symmetry so as to reduce the degeneracy of the ground state and lower its energy.

Table 1 also gives the average equilibrium bond length $R_{M—Rh}$ of the surface Rh and central M atoms. As compared with the interatomic spacing of 0.27 nm for a fcc Rh crystal, obviously, there is a bond length contraction effect in all MRh_{12} clusters, including the $RhRh_{12}$ cluster. Such a contraction effect was observed by extended X-ray-absorption fine structure in Cu and Ni clusters, and the contraction ratio was found to be proportional to the surface-to-volume ratio of the cluster [29], so it is believed to be a reflection of the surface effect.

In order to compare the relative stability of genuine $RhRh_{12}$ and a doped MRh_{12} cluster, we define the binding energy E_b of MRh_{12} clusters at the respective equilibrium configuration as: $E_b(MRh_{12}) = E_{total}(MRh_{12}) - 12E(Rh) - E(M)$. The binding energy for optimized MRh_{12} clusters are also listed in Table 1. From this table, we can easily find that $NiRh_{12}$ is the most energetically stable cluster among all MRh_{12} clusters and all the doped MRh_{12} clusters are more stable than the genuine $RhRh_{12}$ cluster.

Based on the optimized geometrical structures obtained above, we further discuss the electronic and magnetic properties of MRh_{12} clusters. Figs. 2 (*a*), (*b*), 3 (*a*), (*b*), 4 (*a*), (*b*), and 5 (*a*), (*b*) show the partial density of states (PDOS) for the majority-spin and minority-spin electrons of the central M and surface Rh atoms for MRh_{12} clusters respectively. From these figures, we can see that PDOS of the surface Rh and central M atoms for MRh_{12} clusters is mainly contributed by *d* electrons, but the composition of *s* and *p* electrons also can be seen from these figures. Meanwhile, we can also find that the PDOS figures of the surface Rh and central M atoms for all MRh_{12} clusters look similar: there are two

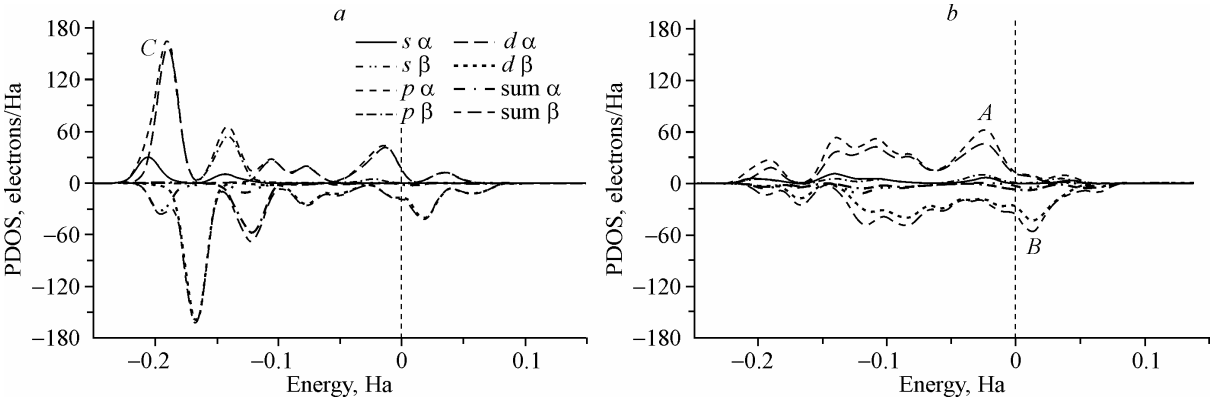

Fig. 2. (*a*) PDOS of central Rh atom for RhR_{12} cluster; (*b*) PDOS of surface Rh atom for RhR_{12} cluster

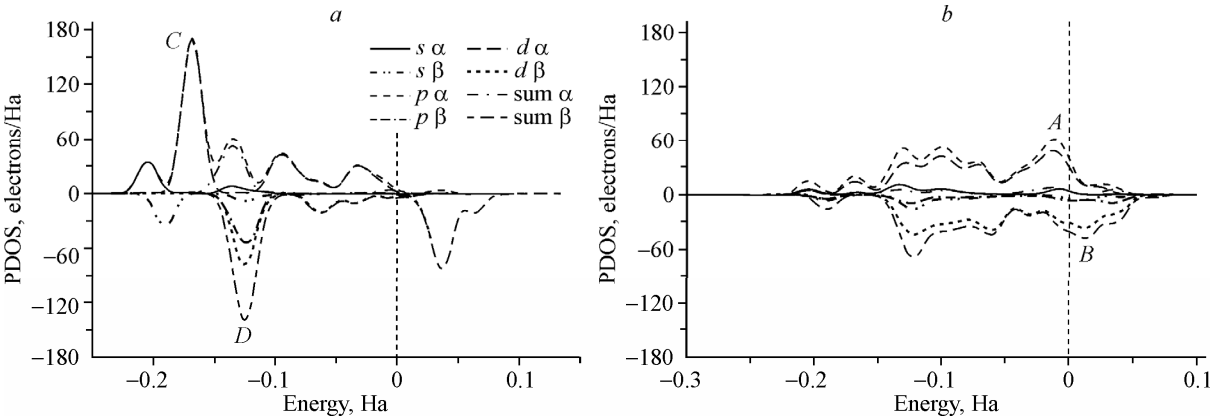

Fig. 3. (*a*) PDOS of central Fe atom for FeR_{12} cluster; (*b*) PDOS of surface Rh atom for FeR_{12} cluster

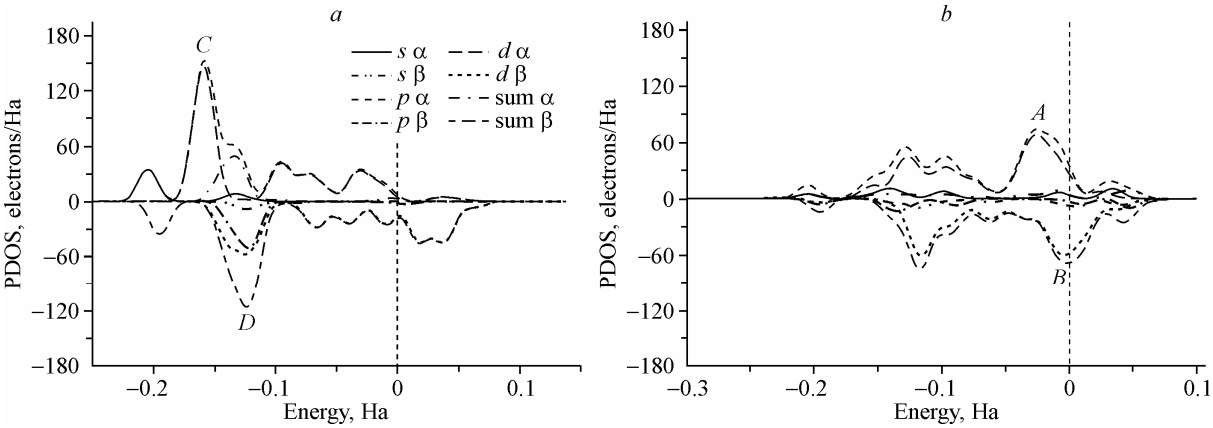

Fig. 4. (*a*) PDOS of central Co atom for CoR_{12} cluster; (*b*) PDOS of surface Rh atom for CoR_{12} cluster

peaks A, B near E_F for the surface Rh atom and two large peaks C, D in the valence band for the central M atom.

However, some differences among these PDOS figures still can be found. For the surface Rh atom, PDOS are mainly of the *d* character; the peak A for majority-spin electrons of $RhRh_{12}$, $FeRh_{12}$, and $NiRh_{12}$ clusters is in the valence band near E_F, and the peak B for minority-spin electrons of $RhRh_{12}$, $FeRh_{12}$, and $NiRh_{12}$ clusters are in the conduction band, but for the $CoRh_{12}$ cluster, peaks A

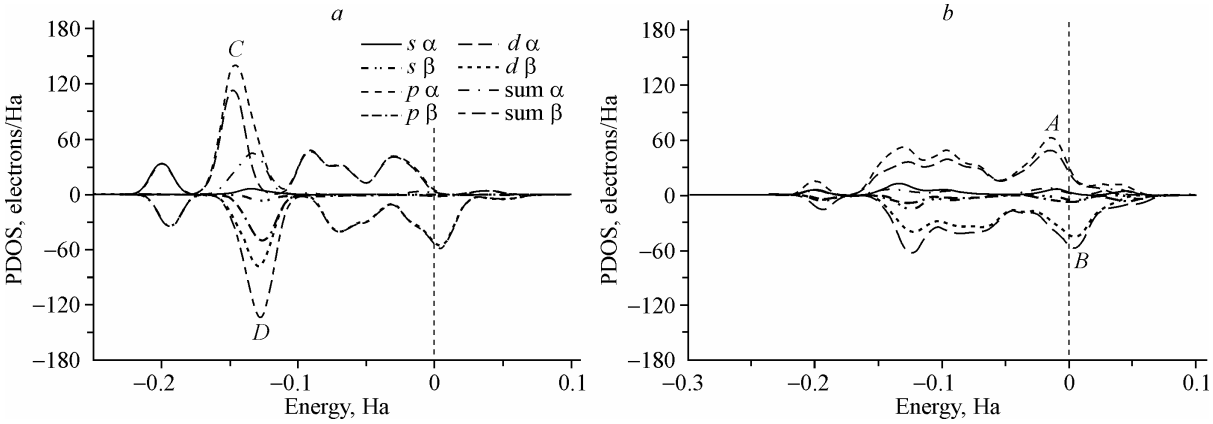

Fig. 5. (*a*) PDOS of central Ni atom for NiR_{12} cluster; (*b*) PDOS of surface Rh atom for NiR_{12} cluster

and B are in the valence band. By comparing the peaks A and B of the surface Rh atom for MRh_{12} clusters, we can find that the exchange splitting of surface Rh atoms for $FeRh_{12}$, $CoRh_{12}$, and $NiRh_{12}$ clusters are smaller than that of the $RhRh_{12}$ cluster. This indicates that the doping M atom has the effect of reducing the exchange splitting of surface Rh atoms to some extent. For the central M atom, peaks C and D of the $RhRh_{12}$ cluster are mainly of the *d* character; for FeRh12 cluster, the peak C is also dominantly of the *d* character, but the peak D is of the *spd* hybrid character. For $CoRh_{12}$ and $NiRh_{12}$ clusters, peaks C and D are obviously of the *spd* hybrid character. With the M substitution for the central Rh atom, PDOS for the central atom have the tendency of changing from the *d* to *spd* hybrid character. In addition, from these figures, we can also see that PDOS of the central M atom above the Fermi energy level for $FeRh_{12}$, $CoRh_{12}$, and $NiRh_{12}$ clusters are almost contributed by minority-spin electrons completely.

Table 2 lists some results of the electronic structure of MRh_{12} clusters. From these data we can find that the gap between the highest occupied molecular orbital (HOMO) and the lowest unoccupied molecular orbital (LUMO) is rather small for all MRh_{12} clusters. Electrons in the valence band can be easily excited to the conduction band; this demonstrates that all MRh_{12} clusters have the metallic character. The values of E_F, E_{HOMO}, E_{LUMO}, and the valence-band width (VBW) for MRh_{12} clusters vary little with M.

For a cluster, the number of electrons in the HOMO determines its ground-state electronic configuration. From the orbital occupation analysis, we can find that the HOMO for $FeRh_{12}$ and $NiRh_{12}$ clusters are fully occupied by the majority-spin and minority-spin electrons, which leads to the ground state with the closed electronic shell, and are remarkably stable. The HOMO for $RhRh_{12}$ and $CoRh_{12}$ clusters are occupied partially only by minority-spin electrons and have open electronic shells. According to the Jahn—Teller theorem, these clusters have the tendency to further distortion to lower symmetry so as to reduce their degeneracy and lower their energy, however, we must point out that the distorted cluster may also increase its degeneracy and have high spin multiplicity if it possesses a de-

Table 2

Data on the electronic structure of MRh_{12} *clusters*

Cluster	VBW, (eV)	HOMO, (eV)	LUMO, (eV)	E_F, (eV)	GAP, (eV)	Electronic configuration
$RhRh_{12}$	6.22	–3.850	–3.648	–3.847	0.202	open
$FeRh_{12}$	6.30	–3.996	–3.982	–3.989	0.014	closed
$CoRh_{12}$	6.15	–4.137	–3.925	–3.964	0.212	open
$NiRh_{12}$	6.05	–3.972	–3.926	–3.957	0.046	closed

creased total energy. This depends on a compromise between the decreasing total energy and increasing degeneracy.

Because the surface Rh atom at a nonequivalent site might have different charge and different magnetic moment, Table 3 specifies these differences between the upper (lower) pentagon Rh and upper (lower) peak Rh atoms. For the $RhRh_{12}$ cluster, all surface Rh atoms have a negative effective charge and the upper (lower) pentagon Rh atom contributes more magnetic moment than the upper (lower) peak Rh atom. For $FeRh_{12}$, $CoRh_{12}$ and $NiRh_{12}$ clusters, the upper (lower) pentagon Rh atom have a negative effective charge, but the upper (lower) peak Rh atom has positive effective charges. The upper (lower) peak Rh atom contributes more magnetic moment than the upper (lower) pentagon Rh atom; the magnetic moment of all surface Rh atoms for $FeRh_{12}$, $CoRh_{12}$, and $NiRh_{12}$ clusters is smaller than that of the surface Rh atom of the $RhRh_{12}$ cluster. Table 4 gives the Mulliken populations and magnetic moments for

Table 3

Charges and magnetic moment of the surface Rh *atom at the nonequivalent site for* MRh_{12} *clusters*

Cluster	Surface Rh atom			
	Upper (lower) pentagon site		Upper (lower) peak site	
	Charge	Magnetic moment	Charge	Magnetic moment
$RhRh_{12}$	–0.054	1.264	–0.004	1.240
$FeRh_{12}$	–0.065	0.705	0.005	0.790
$CoRh_{12}$	–0.049	0.642	0.006	0.729
$NiRh_{12}$	–0.042	0.581	0.029	0.652

Table 4

Mulliken atomic charges and magnetic moment of MRh_{12} *clusters*

Cluster	Surface atom			Central atom			
	Orbital	Charge	Magnetic moment	Orbital	Charge	Magnetic moment	Total
$RhRh_{12}$	4*s*	0.003	0.000	4*s*	0.005	0.000	
	4*p*	0.004	–0.001	4*p*	0.010	–0.001	
	4*d*	0.002	1.179	4*d*	0.289	1.090	
	5*s*	0.160	0.057	5*s*	0.391	–0.017	
	5*p*	–0.215	0.023	5*p*	–0.147	0.017	
		–0.046	1.260		0.548	1.089	16
$FeRh_{12}$	4*s*	–0.001	0.000	3*s*	–0.005	–0.003	
	4*p*	0.006	0.000	3*p*	–0.007	–0.011	
	4*d*	–0.019	0.690	3*d*	–0.452	3.270	
	5*s*	0.161	0.015	4*s*	1.507	0.018	
	5*p*	–0.200	0.014	4*p*	–0.411	0.060	
		–0.053	0.719		0.632	3.334	12
$CoRh_{12}$	4*s*	0.003	0.000	3*s*	–0.002	–0.002	
	4*p*	0.003	0.000	3*p*	–0.009	–0.008	
	4*d*	–0.008	0.626	3*d*	–0.611	2.069	
	5*s*	0.161	0.020	4*s*	1.504	0.003	
	5*p*	–0.199	0.011	4*p*	–0.409	0.027	
		–0.040	0.657		0.473	2.089	10
$NiRh_{12}$	4*s*	0.003	0.000	3*s*	0.003	0.000	
	4*p*	0.004	0.000	3*p*	–0.006	–0.002	
	4*d*	–0.020	0.568	3*d*	–0.650	0.894	
	5*s*	0.182	0.024	4*s*	1.411	–0.010	
	5*p*	–0.199	0.009	4*p*	–0.392	–0.001	
		–0.030	0.592		0.366	0.881	8

different atomic orbitals of MRh_{12} clusters; the results for the surface Rh atom given in Table 3 are the average value. From these tables, we can see that the central M atom has a positive effective charge, and the surface Rh atom has a negative effective charge in all MRh_{12} clusters. This means, generally speaking, that the surface Rh atoms obtain electrons from the central M atom. For all MRh_{12} clusters, the magnetic moments of the central M atom align in parallel to those of the surface atoms; so they have the ferromagnetic (FM) interaction. This situation is very similar to the result for the Rh_{13} cluster obtained by professor Yang [27]. Among all MRh_{12} clusters, the total magnetic moments of the clusters are reduced by the M substitution for the central Rh atom.

Further analysis indicates that electron transfer may take place between two atomic orbitals of one atom or between two atomic orbitals of different atoms in one cluster. For the $RhRh_{12}$ cluster, charge transfer occurs mainly from Rh 4*s*, 4*p*, 4*d*, 5*s* orbitals to the Rh 5*p* orbital not only for the central Rh atom, but also for surface Rh atoms. For the surface Rh 4*d* orbital, charge transfer is very small. This indicates that the *spd* hybrid effect for the surface Rh 4*d* orbit is not very significant; the unpaired *d* electrons in surface Rh 4*d* orbitals are also not easy to be paired, so the magnetic moment of the $RhRh_{12}$ cluster is mainly contributed by Rh 4*d* orbitals. For MRh_{12} (M = Fe, Co, and Ni) clusters, charges are mainly transferred from the surface Rh 5*s* and central M 4*s* orbitals to the Rh 4*d*, 5*p* and M 3*d*, 4*p* orbitals. Unlike the $RhRh_{12}$ cluster, the surface Rh 4*d* and central M 3*d* orbitals in MRh_{12} clusters do not lose, but obtain electrons. It is well known that for TM clusters, magnetic moments mainly come from the localization of *d* electrons, from Table 4 we can find that, as compared with the $RhRh_{12}$ cluster, more charge is transferred from other orbitals to Rh 4*d* and M 3*d* orbitals. This shows that the *spd* hybrid effect in the *d* orbitals of MRh_{12} clusters is stronger than that in the $RhRh_{12}$ cluster; the unpaired *d* electrons in MRh_{12} clusters have more chance to be paired. The enhancement of *spd* hybridization and delocalization of valence electrons leads to the magnetic shielding that in turn enhances the stability. This effect is also the main reason why the total magnetic moments of MRh_{12} (M = Fe, Co, and Ni) clusters are reduced by the M substitution for the central Rh atom.

CONCLUSIONS

In this paper, we have performed a first principles study on the geometrical structure, electronic and magnetic properties of MRh_{12} clusters. The results we obtained can lead to the following conclusions:

(1) The relative stable geometrical structure of MRh_{12} clusters is not a perfect symmetrical structure, but a distorted one; the bond length contraction is obvious in MRh_{12} clusters and believed to be the reflection of the surface effect.

(2)According to our calculation, the binding energy for MRh_{12} clusters is larger than that of the $RhRh_{12}$ cluster; this indicates that heterogeneous doped MRh_{12} clusters are more stable than the genuine $RhRh_{12}$ cluster.

(3) The effect of the impurity M on the density of states, valence band width, Fermi energy level, HOMO and LUMO for MRh_{12} clusters is not significant, but with the M substitution for the central Rh atom the magnetic moment of MRh_{12} is dramatically reduced.

(4) Mulliken populations indicate that the surface Rh atoms obtain electrons from the central M atom for all MRh_{12} clusters;the moments of the central M atom align in parallel to those of the surface atoms, so they have ferromagnetic (FM) interaction. Further analysis indicates that more charge is transferred from other orbitals to Rh 4*d* and M 3*d* orbitals, and the *spd* hybrid effect in the *d* orbitals of MRh_{12} clusters is stronger than that in the $RhRh_{12}$ cluster. This situation means that the unpaired *d* electrons will have more chance to be paired; this is the reason why the magnetic moments of MRh_{12} clusters are reduced.

Acknowledgements. This work is supported by the Nature Science Foundation of Chongqing city. No. CSTC-2007BB4137.

REFERENCES

1. *Quinonero D., Garura C., Frontera A. et al.* // J. Phys. Chem. A. – 2005. – **109**. – P. 4632 – 4637.
2. *Reddy S., Sastry G.N.* // Phys. Chem. A. – 2005. – **109**. – P. 8893 – 8903.
3. *Gpeev A., Yang C., Klippenstein S.J., Dunbar R.C.* // Phys. Chem. A. – 2000. – **104**. – P. 3246 – 3256.
4. *Quinn D.M., Feaster S.R., Nair H.K. et al.* // J. Amer. Chem. Soc. – 2000. – **122**. – P. 2975 – 2980.
5. *Armentrout P.B., Rodgers M.T.* // Phys. Chem. A. – 2000. – **104**. – P. 2238 – 2247.
6. *Huang H., Rodgers M.T.* // Phys. Chem. A. – 2002. – **106**. – P. 4277 – 4289.
7. *Garura C., Frontera A., Quinonero D. et al.* // J. Phys. Chem. A. – 2004. – **108**. – P. 9423 – 9427.
8. *Gal J., Maria P., Decouzon M., Abboud J.L.M.* // Amer. Chem. Soc. – 2003. – **125**. – P. 10394 – 10401.
9. *Garura C., Frontera A., Quinonero D. et al.* // Chem. Phys. Lett. – 2003. – **382**. – P. 534 – 540.
10. *Guell M., Poater J., Luis J.M., Sola M.* // Chem. Phys. Chem. – 2005. – **6**. – P. 2552 – 2561.
11. *Rinza T.R., Trujillo J.H.* // Chem. Phys. Lett. – 2006. – **422**. – P. 36 – 40.
12. *Beene L., Brandt G.S., Zhong W. et al.* // Biochemistry. – 2002. – **41**. – P. 10262 – 10269.
13. *Boys S.F., Bernardi F.* // Mol. Phys. – 1970. – **19**. – P. 553 – 566.
14. *Frisch M.J., Trucks G.W., Schlegel H.B., Scuseria G.E., Robb M.A., Cheeseman J.R., Montgomery J.A. Jr., Vreven T., Kudin K.N., Burant J.C., Millam J.M., Iyengar S.S., Tomasi J., Barone V., Mennucci B., Cossi M., Scalmani G., Rega N., Petersson G.A., Nakatsuji H., Hada M., Ehara M., Toyota K., Fukuda R., Hasegawa J., Ishida M., Nakajima T., Honda Y., Kitao O., Nakai H., Klene M., Li X., Knox J.E., Hratchian H.P., Cross J.B., Adamo C., Jaramillo J., Gomperts R., Stratmann R.E., Yazyev O., Austin A.J., Cammi R., Pomelli C., Ochterski J.W., Ayala P.Y., Morokuma K., Voth G.A., Salvador P., Dannenberg J.J., Zakrzewski V.G., Dapprich S., Daniels A.D., Strain M.C., Farkas O., Malick D.K., Rabuck A.D., Raghavachari K., Foresman J.B., Ortiz J.V., Cui Q., Baboul A.G., Clifford S., Cioslowski J., Stefanov B.B., Liu G., Liashenko A., Piskorz P., Komaromi I., Martin R.L., Fox D.J., Keith T., Al-Laham M.A., Peng C.Y., Nanayakkara A., Challacombe M., Gill P.M.W., Johnson B., Chen W., Wong M.W., Gonzalez C., Pople J.A.* Gaussian, Inc., Pittsburgh PA, 2003.
15. *Reed E., Curtiss L.A., Weinhold F.* // Chem. Rev. – 1988. – **88**. – P. 899 – 926.
16. *Glendening D., Reed A.E., Carpenter J.E., Weinhold F.* NBO Version 3.1.
17. *Bader R.F.W.* Hamilton, McMaster University, 2000.
18. *Cubero E., Orozco M., Luque F.J.* // Proc. Natl. Acad. Sci. USA. – 1998. – **95**.